J Nanopart Res (2013) 15:2000
DOI 10.1007/s11051-013-2000-z

RESEARCH PAPER

Multiparameter-dependent spontaneous emission in PbSe quantum dot-doped liquid-core multi-mode fiber

Lei Zhang · Yu Zhang · Hua Wu · Tieqiang Zhang · Pengfei Gu · Hairong Chu · Tian Cui · Yiding Wang · Hanzhuang Zhang · Jun Zhao · William W. Yu

Received: 17 June 2013 / Accepted: 5 September 2013 / Published online: 25 September 2013

Abstract A theoretical model was established in this paper to analyze the properties of 3.50 and 4.39 nm PbSe quantum dot-doped liquid-core multi-mode fiber. This model was applicable to both single- and multi-mode fiber. The three-level system-based light-propagation equations and rate equations were used to calculate the guided spontaneous emission spectra. Considering the multi-mode in the fiber, the normalized intensity distribution of transversal model was improved and simplified. The detailed calculating results were thus obtained and explained using the above-mentioned model. The redshift of the peak position and the evolution of the emission power were observed and analyzed considering the influence of the fiber length, fiber diameter, doping concentration, and the pump power. The redshift increased with the increases of fiber length, fiber diameter, and doping concentration. The optimal fiber length, fiber diameter, and doping concentration were analyzed and confirmed, and the related spontaneous emission power was obtained. Besides, the normalized emission intensity increased with the increase of pump power in a nearly linear way. The calculating results fitted well to the experimental data.

Keywords PbSe · Quantum dots · Liquid-core · Fiber

Introduction

There has been a rapid development in semiconductor quantum dots (QDs) because of their unique electrical

L. Zhang · Y. Zhang (✉) · H. Wu · Y. Wang · W. W. Yu (✉)
State Key Laboratory on Integrated Optoelectronics, and College of Electronic Science and Engineering, Jilin University, Changchun 130012, China
e-mail: yuzhang@jlu.edu.cn

W. W. Yu
e-mail: wyu6000@gmail.com

L. Zhang · Y. Zhang · T. Zhang · P. Gu · T. Cui · H. Zhang (✉)
College of Physics, and State Key Laboratory of Superhard Materials, Jilin University, Changchun 130012, China
e-mail: zhanghz@jlu.edu.cn

H. Chu
Changchun Institute of Optics, Fine Mechanics and Physics, Chinese Academy of Sciences, Changchun 130025, China

J. Zhao · W. W. Yu
College of Material Science and Engineering, Qingdao University of Science and Technology, Qingdao 266042, China

J. Zhao · W. W. Yu
Department of Chemistry and Physics, Louisiana State University, Shreveport, LA 71115, USA

and optical properties. These particles have relatively narrow emission spectra, a broad spectral absorption (Lipovskii et al. 1997), and high quantum efficiency that can reach over 80 % (Du et al. 2002). In addition, the absorption (Abs) and photoluminescence (PL) of QDs (such as CdS, CdSe, CdTe, PbS, PbSe, and PbTe) present strong size-dependent properties which are different from the corresponding bulk materials due to the quantum confinement effect (Yu et al. 2003; Choudhury et al. 2005; Dai et al. 2009) and can be tuned accurately over a wide band. Among the many types of semiconductor QDs, PbSe QDs have become one of the most promising candidates. Their tunable band gap can cover the whole optical fiber communication windows due to the large Bohr radius of 46 nm (approximately eight times larger than that of CdSe (Wise 2000)). Meanwhile, PbSe QDs have recently shown great potentials in telecommunication (Steckel et al. 2003), photo detection (McDonald et al. 2005), biomedical imaging (Weissleder 2001; Medintz et al. 2005), and solar energy conversion (Schaller and Klimov 2004; Ellingson et al. 2005; Koleilat et al. 2008).

PbSe QD-doped fiber has attracted much attention in recent years. Watekar et al. (2010) reported linear and nonlinear optical properties of the PbSe QD-doped germano-silica glass optical fiber. Hreibi et al. (2011) obtained emissions at 1,220 nm with a bandwidth of 120 nm by the injection of a 532 nm pump source into a PbSe QD-doped liquid-core optical fiber. Cheng and Zhang (2007) simulated PbSe QD-doped optical fiber theoretically. It is known that when PbSe QDs are doped into a fiber, the PL spectra of the QD solution show some different properties due to the limitation of the optical waveguide, such as the reabsorption-induced redshift effect and the optimal value of fiber length, fiber diameter, and doping concentration. It is important to investigate the theoretical models of QD-doped fiber to analyze the instinct optical properties. Cheng and Zhang (2007) have done the theoretical calculations comprehensively, including the gain, bandwidth, and noise of PbSe-doped fiber amplifier based on a three-level system which is applicable to the single-mode fiber. Though there are several experimental studies of PbSe QD-doped fiber, few reports focus on the guided spontaneous emission in the QD-doped liquid-core multi-mode fiber.

We report in this paper a theoretical model to simulate and analyze the evolution of the spectra of QD-doped fiber. The model can be generally applied to simulate both single- and multi-mode fiber. Besides, more factors are involved, such as the quantum efficiency of PbSe QDs, the leakage of the fiber, and the non-radiative transition from the generation of multi-exciton. The simulation result was confirmed to agree well with the experimental data in liquid-core QD-doped fiber. This research can be a theoretical basis for the future development of QD-doped multi-mode fiber amplifiers.

Calculation

The QD-doped liquid-core multi-mode fiber was fabricated by using a capillary waveguide of silica dioxide filled with QD solution (PbSe QDs dispersed in tetrachloroethylene) as shown in Fig. 1. When a continuous laser source was coupled into the liquid-core using a convex lens, the QDs in the fiber would be excited and radiate luminescence. The spectra were recorded at the end of fiber. The calculations are based on the ideal theory model in the assumptions of the straight hollow waveguide, the spherical QD shape, the monodisperse size distribution of nanoparticle, and the constant doping concentration. The abs and emission-induced electron–hole transitions are shown in Fig. 2a, in which the E_g is the band gap energy and ^1S_e ^1P_e,^1S_h ^1P_h represent the several lowest electron and hole states (Harbold et al. 2005; Shabaev et al. 2006). When the photon energy absorbed by PbSe QDs is greater than E_g, the electron in the ground state can be excited to the excited state, which correspond to ^1S_h–^1S_e(the first exciton abs peak),^1S_h–^1P_e, ^1P_h–^1S_e, and ^1P_h–^1P_e, etc., respectively, then the electron goes back to the ground state corresponding to^1S_e–^1S_h. It is

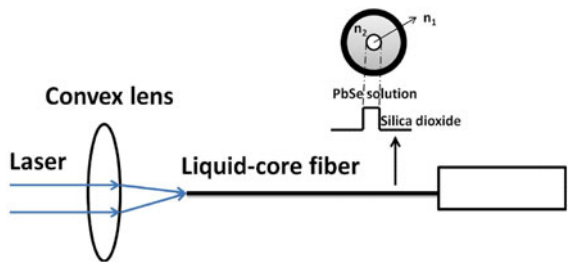

Fig. 1 The schematic diagram of PbSe QD-doped liquid-core fiber. *Inset*: cross section diagram of liquid-core fiber and its equivalent step refractive index profile

noticed that although the transitions of ^1S_h–^1P_e and ^1P_h–^1S_e gain some oscillator strength, they are still orders of magnitude weaker than the transitions of ^1S_h–$^1S_e$and ^1P_h–^1P_e(Liljeroth et al. 2005), so the level diagram can be considered as a three-level system as an approximation shown in Fig. 2b.

Level 1 is the ground state. Level 2 represents the band gap energy and consists of two-fine levels corresponding to both the emission peak and the first abs peak. Level 3 is the higher energy level (Bahrampour et al. 2009; Cheng and Zhang 2007). When PbSe QDs are pumped by a short wavelength light, due to large abs cross section, QDs are excited to populate the upper levels 2 and 3 in a probability W_{12} and W_{13}, namely the stimulated abs probability. The transition from level 1 to level 2 corresponds to ^1S_h–^1S_e in Fig. 2a, the corresponding abs is the first excitonic abs peak; the transition from level 1 to level 3 corresponds to^1S_h–^1P_e, ^1P_h–^1S_e and ^1P_h–^1P_e in Fig. 2a. The population of level 2 comes back to the ground state by two channels, one is the emission with a probability A_{21}, namely the spontaneous emission probability, and another is a non-radiative transition with a probability A_{21}^{NR}, corresponding to the transition of ^1S_e–^1S_h The energy absorbed by QDs is higher than that the emitted due to the size distribution (Lifshitz et al. 2006), the Coulomb interaction between the electron and hole (An et al. 2007), and the Frank–Condon effect (Franceschetti 2008) which lead to Stokes shift (Leitsmann and Bechstedt 2009). The population of level 3 de-excites to level 2 by the non-radiative transition with a probability A_{32}^{NR}, corresponding to the transition of ^1P_e–^1S_e, and then to the ground state by the emissive or non-radiative transitions (A_{21} or A_{21}^{NR}). It is worth noticing that when the PbSe QDs/tetrachloroethylene were filled into a hollow fiber and excited by a continuous laser, the population of level 2 can also come back to the ground state by the emission with a probability W_{21} as shown in Fig. 2b. Therefore, the emission can be generated and can transmit along the liquid-core fiber because of the total reflection; That is, the mechanism of the guided spontaneous emission in the liquid-core QD-doped fiber. It should be noticed that the pump source with a high power can normally create more than one excitons per dot and the deactivation of multi e–h pair states in nanocrystals is dominated by non-radiative Auger recombination (Klimov 2006) which is also considered in our theory model.

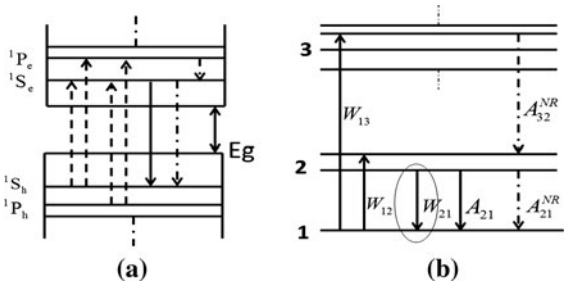

Fig. 2 **a** The diagram of energy level in PbSe QDs including absorption (*upward dotted lines*), emission (*solid line*), and non-radiative transitions (*downward dotted lines*). **b** The three-level structure diagram of PbSe quantum dot

The rate equations for the three-level system are employed for the theoretical calculation.

$$\frac{dn_1}{dt} = -(W_{13} + W_{12})n_1 + \left(W_{21} + A_{21} + A_{21}^{NR}\right)n_2 \tag{1a}$$

$$\frac{dn_2}{dt} = W_{12}n_1 - \left(W_{21} + A_{21} + A_{21}^{NR}\right)n_2 + A_{32}^{NR}n_3 \tag{1b}$$

$$\frac{dn_3}{dt} = W_{13}n_1 - A_{32}^{NR}n_3 \tag{1c}$$

$$n_t = n_1 + n_2 + n_3 \tag{1d}$$

where n_1, n_2, n_3, and n_t are the population densities of levels 1, 2, 3, and all the three levels, respectively. Then, the two following situations are considered in order to achieve the population distribution in the three levels.

1) Steady-state approximation $(dn_i/dt = 0,\ i = 1, 2, 3)$;

The transition time of particles from level 3 to level 2 is very short, so the probability of non-radiative transition is much higher than that of the pump, i.e., $A_{32}^{NR} > > W_{13}$, some research work have also reported that level 3 has a very short fluorescence lifetime ($\tau_3 = 1/A_{32}^{NR} \leq 6$ps (Wehrenberg et al. 2002; Harbold et al. 2005), τ_3 is the relaxation time of the transition from level 3 to level 2). Therefore, the population of level 3 transits immediately down to level 2, resulting in the degradation from three-level system to two-level system.

Therefore, the Eqs. (1a), (1b), and (1c) can be written as:

$$n_1 = n_t \frac{\left(1 + W_{21}\tau_R + \frac{\tau_R}{\tau_{NR}}C\right)}{1 + \tau_R\left(W_{21} + W_{12} + W_{13} + \frac{C}{\tau_{NR}}\right)} \tag{2a}$$

$$n_2 = n_t \frac{(W_{13} + W_{12})\tau_R}{1 + \tau_R\left(W_{21} + W_{12} + W_{13} + \frac{C}{\tau_{NR}}\right)} \tag{2b}$$

$$n_3 = n_t - n_1 - n_2 \tag{2c}$$

where $\tau_R = 1/A_{21}$ is the lifetime of spontaneous radiation, τ_{NR} is the lifetime of non-radiative emission and can be written as (Klimov 2006) $\tau_{NR} = \left(C_A n_{eh}^2\right)^{-1}$ where n_{eh} is the carrier concentration ($n_{eh} = N/V$), N is the number of the generated excitons per QD. $\langle N\rangle = j_p \sigma_a(\nu_p)$ and $C_A = \beta_A (D/2)^3$, where $\beta_A = 2.69$ ps^{-1} nm^3 for PbSe QDs, D is the QD diameter, $\sigma_a(\nu_p)$ is the abs cross section of the pump, j_p is the pump fluence measured in photons/cm^2, V is the average volume of one QD particle, and C is the proportion of the non-radiative and radiative transition.

The probability $W_{21}(\nu)$ is in proportion to the emission intensity $I_{\nu_s}(r,z)$ and the emission cross section $\sigma_e(\nu_s)$ (Peterka et al. 2004; Giles and Desurvire 1991); therefore, the probabilities of the emission and the abs can be given as follows,

$$W_{21}(r,z) = \sum_{\nu_s=\nu_1}^{\nu_m} \frac{\sigma_e(\nu_s)}{h\nu_s} p_{\nu_s}(z) i_{\nu_s}(r) \tag{3a}$$

$$W_{12}(r,z) = \sum_{\nu_s=\nu_0}^{\nu_m} \frac{\sigma_a(\nu_s)}{h\nu_s} p_{\nu_s}(z) i_{\nu_s}(r) \tag{3b}$$

$$W_{13}(r,z) = \frac{\sigma_a(\nu_p)}{h\nu_p} p_{\nu_p}(z) i_{\nu_p}(r) \tag{3c}$$

where h is the Planck constant, ν_s and ν_p are frequencies of spontaneous emission and the pump, ν_0 and ν_1 are the minimal frequencies of the abs and the emission, and ν_m represents the maximal one. $i_{\nu_s}(r)$ and $i_{\nu_p}(r)$ are the normalized intensity distribution of transversal model; $\sigma_a(\nu_s)$ and $\sigma_e(\nu_s)$ are the abs and emission cross sections of the spontaneous emission and can be obtained according to Lambert–Beer's law (Dai et al. 2009) and the theory of McCumber (McCumber 1964). P_{ν_s} and P_p represent the power of spontaneous emission and pump source.

Substituting (3a), (3b), and (3c) in (2a) and (2b), the relationship between the population distribution of level 1 and level 2 and the light power in the optical fiber can be expressed as

$$n_1 = n_t \frac{1 + \sum_{\nu_s=\nu_1}^{\nu_m} \frac{\sigma_e(\nu_s)}{h\nu_s}\tau_R i_{\nu_s}(r) P_{\nu_s}(z) + \frac{\tau_R}{\tau_{NR}}C}{1 + \tau_R\left[\sum_{\nu_s=\nu_1}^{\nu_m} \frac{\sigma_e(\nu_s)}{h\nu_s} i_{\nu_s}(r) P_{\nu_s}(z) + \sum_{\nu_s=\nu_0}^{\nu_m} \frac{\sigma_a(\nu_s)}{h\nu_s} i_{\nu_s}(r) P_{\nu}(z) + \frac{\sigma_a(\nu_p)}{h\nu_p} i_{\nu_p}(r) P_p(z)\right] + \frac{\tau_R}{\tau_{NR}}C} \tag{4a}$$

$$n_2 = n_t \frac{\tau_R\left(\frac{\sigma_a(\nu_p)}{h\nu_p} i_{\nu_p}(r) P_p(z) + \sum_{\nu_s=\nu_0}^{\nu_m} \frac{\sigma_a(\nu_s)}{h\nu_s} i_{\nu_s}(r) P_{\nu_s}(z)\right)}{1 + \tau_R\left[\sum_{\nu_s=\nu_1}^{\nu_m} \frac{\sigma_e(\nu_s)}{h\nu_s} i_{\nu_s}(r) P_{\nu_s}(z) + \sum_{\nu_s=\nu_0}^{\nu_m} \frac{\sigma_a(\nu_s)}{h\nu_s} i_{\nu_s}(r) P_{\nu_s}(z) + \frac{\sigma_a(\nu_p)}{h\nu_p} i_{\nu_p}(r) P_p(z)\right] + \frac{\tau_R}{\tau_{NR}}C} \tag{4b}$$

The variations of the emission along z-axis can be explained in four parts,

$$\frac{dP_{\nu_s}}{dz} = \frac{dP_{spon}}{dz} + \frac{dP_{sti-emission}}{dz} + \frac{dP_{sti-abs}}{dz} + \frac{dP_{fiberloss}}{dz} \tag{5}$$

The four terms represent the spontaneous emission, the stimulated emission, the stimulated abs, and the excess fiber loss, respectively.

$$\frac{dp_{spon}}{dz} = \sigma_e(\nu_s) \int_0^R i_{\nu_s}(r)\, n_2(r,z)[mh\nu_s \Delta\nu_s] 2\pi r dr \tag{6a}$$

$$\frac{dP_{sti-emission}}{dz} = \sigma_e(v_s)\int_0^R i_{v_s}(r)\, n_2(r,z)[P_{vs}(z)]2\pi r dr \tag{6b}$$

$$\frac{dP_{sti-abs}}{dz} = -\sigma_a(v_s)\int_0^R i_{v_s}(r) n_1(r,z) P_{vs}(z) 2\pi r dr \tag{6c}$$

$$\frac{dP_{fiberloss}}{dz} = -l_v P_{vs}(z) \tag{6d}$$

Similarly, the variations of the pump light along z-axis can be expressed as the stimulated abs by QDs and the excess fiber loss.

$$\frac{dP_p}{dz} = \frac{dP_{abs}}{dz} + \frac{dP_{fiberloss}}{dz} \tag{7}$$

$$\frac{dP_{abs}}{dz} = -\sigma_a(v_p)\int_0^R i_{v_p}(r) n_1(r,z) P_p(z) 2\pi r dr \tag{8a}$$

$$\frac{dP_{fiberloss}}{dz} = -l_v P_p(z) \tag{8b}$$

Therefore, the power propagation equations that describe the propagation of spontaneous emission and pump power in the liquid-core fiber can be given as

$$\frac{dP_{vs}(z)}{dz} = \sigma_e(v_s)\int_0^R i_{v_s}(r) n_2(r,z)[P_{vs}(z) + mhv_s\Delta v_s]2\pi r dr - \sigma_a(v_s)\int_0^R i_{v_s}(r) n_1(r,z) P_{vs}(z) 2\pi r dr - l_v P_{vs}(z) \tag{9a}$$

$$\frac{dP_p(z)}{dz} = -\sigma_a(v_p)\int_0^R i_{v_p}(r) n_1(r,z) P_p(z) 2\pi r dr - l_v P_p(z) \tag{9b}$$

where l_v is the excess fiber loss per length, Δv_s is the effective noise bandwidth, m is the number of modes, and R is the radius of fiber core. On the right side of Eq. 9a, the first term is from the emission, the second term is from the abs loss, and the last term is from the excess fiber loss including scattering loss, solution abs, light escape loss, etc.

The normalized intensity distribution of transversal model i_v (r) with a frequency v is improved and simplified so as to avoid the restriction of single-mode fiber and is deduced in detail. The distribution of the emission power along the radial direction satisfies the zero-order Bessel function and can be expressed as

$$P_s(r_j v) = \left[\frac{J_0(V_j)}{J_0(V_1)}\right]^2 P_s(r_1) \tag{10}$$

where V_j is the normalized frequency and is represented as

$$V_j = \frac{2\pi}{\lambda}\sqrt{n_{core}^2 - n_{clad}^2}\, r_j \tag{11}$$

where n_{core} and n_{clad} are the refractive indexes of the core and the clad of the fiber, respectively. The integral of Eq. (10) can be expressed as

$$P_s(v) = \int_0^R P_s(r_j, v) r dr d\theta = \frac{P_s(r_1)}{[J_0(V_1)]^2}\int_0^R [J_0(V)]^2 r dr d\theta \tag{12}$$

The normalized intensity distribution of transversal model can be written as

$$i(r) = \frac{P_s(r_j, v)}{P_s(v)} = \frac{[J_0(V)]^2}{\int [J_0(V)]^2 r dr d\theta} = \frac{[J_0(V)]^2}{2\pi\int_0^R [J_0(V)]^2 r dr} \tag{13}$$

Equation (13) can be employed to avoid the restriction of single-mode fiber. Substituting (4a) and (4b) in (9a) and (9b), the evolution of the spontaneous emission power can be achieved under different fiber lengths, fiber diameters, pump powers, and doping concentrations.

Results and discussion

Spectral properties of liquid-core fiber can be obtained and analyzed through the above-mentioned theory model and formulas considering the influence of some important factors. PbSe QDs with particle size of 4.39 nm (as shown in Fig. 3b) were prepared according to the method reported by Yu et al. (2004). The abs and PL spectra of PbSe QD solution were the record for the calculation of the abs and emission cross

section (Fig. 3a). The abs and emission peaks locate at 1,378 and 1,452 nm, respectively. The refractive indexes used for the theoretical calculation for n_{clad} and n_{core} were 1.45 and 1.505, respectively.

Figure 4a shows the calculated evolution of the fiber length-dependent spontaneous emission output power and the pump output power with a doping concentration of $4 \times 10^{21}/m^3$, fiber diameter of 100 μm, and pump power of 60 mW. A maximum output of the emission power was confirmed at the fiber length of 15 cm where the pump output was close to zero. Figure 4b shows the calculated emission spectra under different fiber lengths (5–70 cm) when the parameters are the same as the ones in Fig. 4a. Figure 4c, d are the normalized fiber length-dependent spontaneous emission power and peak position, respectively. It can be seen that: (1) the peak position shifts to red with the increase of the fiber length and (2) the optical output power increases with the increase of the fiber length from 5 to 15 cm and then decreases when the fiber length is longer than 15 cm, indicating a maximum of emission intensity at a fiber length of

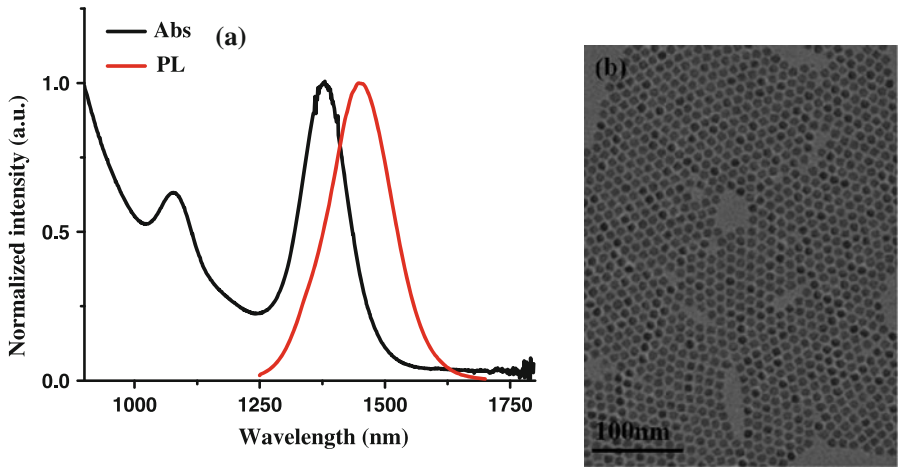

Fig. 3 **a** Absorption and photoluminescence spectra of PbSe QDs. **b** TEM image of 4.39 nm PbSe QDs

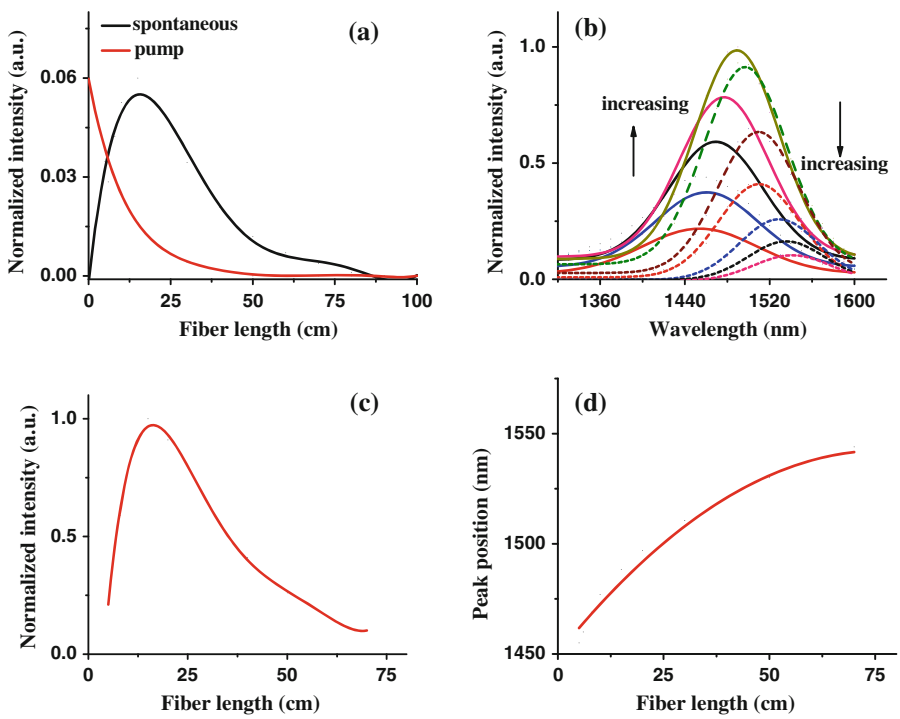

Fig. 4 **a** The evolution of the spontaneous emission power and pump power with the fiber length change. **b** The calculated emission spectra under different fiber lengths (5–70 cm) in which the directions of the *arrows* represent the increase of the fiber length from 5 to 6, 8, 10, 15, 20, 30, 40, 50, 60, and 70 cm. **c**, **d** The normalized fiber length-dependent emission power and peak position, respectively

15 cm. The redshift can be explained primarily by an overlap between the abs spectrum and the emission band of the particles (see Fig. 3). The generated emission by relatively smaller QD particles can be reabsorbed by the relatively larger QD particles at this particle contribution and the long light path (up to 75 cm in this study) (although the synthesized PbSe QDs could be regarded as monodisperse in particle size, there was still a size distribution of 6 %). Thus, the emission contribution from the shorter wavelength will be weakened and the output spectra of fiber shift to red compared to QD spectra. This is the so-called reabsorption–emission effect. Longer fiber length leads to more serious reabsorption–emission, and, therefore, more redshift. Additionally, when the optical fiber length reaches a certain value, the pump light will be completely absorbed and the decreased population of the upper level induces the reduction of the spontaneous emission. Therefore, an optimal fiber length was observed.

Figure 5 shows the variation of fiber diameter-dependent emission spectra, normalized spontaneous emission power, and peak position for a 15-cm-long fiber with a doping concentration of $4 \times 10^{21}/m^3$ and a pump power of 60 mW. It can be seen that: (1) the peak position shifts to red with the increase of the fiber diameter and (2) the output power increases with the increase of the fiber diameter first and then decreases when the diameter is larger than 60 μm. Since the number of PbSe QD particles in large-diameter fiber is more than that in small-diameter fiber leading to higher probability of reabsorption-emission, the redshift is more obvious for large-diameter fiber. Similar to the fiber length change, when the fiber diameter increases to a certain value, there are enough QD particles to absorb the pump light completely and, therefore, the population of the upper level reduces, which causes the decrease of the spontaneous emission. Consequently, an optimal fiber diameter would exist.

Figure 6 shows the calculations for doping concentration-dependent emission spectra, normalized spontaneous emission power, and peak position for a 15-cm fiber with 100 μm diameter and pump power of 60 mW. It can be seen that: (1) the redshift becomes obvious with the increase of the doping concentration and (2) there is a maximum of emission and the corresponding doping concentration is $4 \times 10^{21}/m^3$. The redshift is related to the above-mentioned reabsorption–emission effect. Higher concentration leads to stronger reabsorption–emission, and hence results in the larger redshift. When the pump power is fixed, the maximum population of the upper level is a constant. Therefore, the total population increases and the spontaneous emission rises with higher doping concentration when the QD concentration is not too high. However, when the QD concentration is higher than a certain value, the population will not increase anymore because of the limited pump power. The QD radiation will be reabsorbed and scattered by the excess particles, which subsequently induces the decline of the emission intensity.

Figure 7 depicts the evolution of the pump power-dependent emission spectra and the normalized spontaneous power in a 15-cm fiber with a diameter of 100 μm and a doping concentration of $4 \times 10^{21}/m^3$. The spontaneous emission increases with the increase of pump power in a nearly linear way (about 0.0098/mW) because of the enhanced population of the level 2.

In order to analyze the practicability of this theoretical model, the experimental results reported

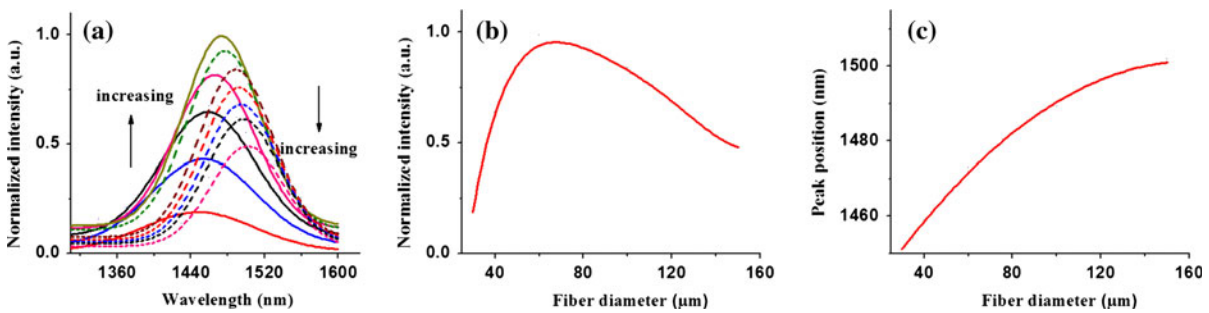

Fig. 5 **a** The calculated spontaneous emission spectra under different fiber diameters (10–100 μm) in which the directions of the *arrows* represent the increase of the fiber diameter from 30 to 35, 40, 50, 60, 70, 100, 110, 120, 130, and 140 μm. **b**, **c** The normalized fiber diameter-dependent emission power and peak position, respectively

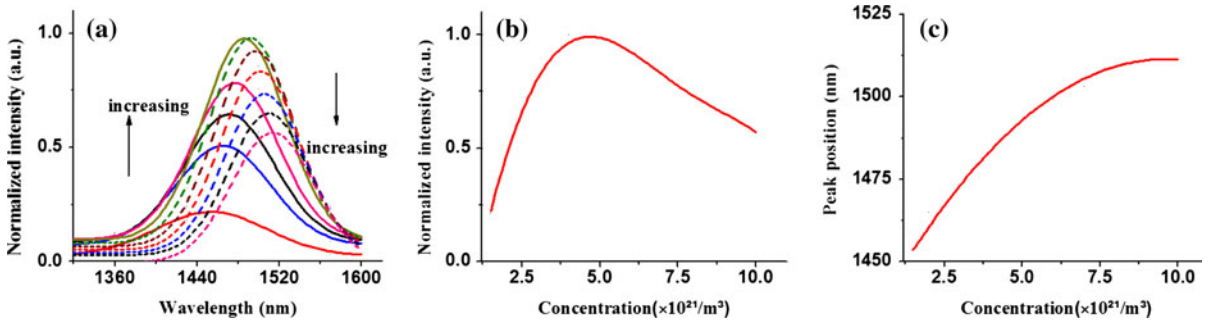

Fig. 6 **a** The calculated spontaneous emission spectra under different doping concentrations in which the directions of *arrows* represent the increase of doping concentration from 1.5 to 2, 2.5, 3, 4, 5, 6, 7, 8, 9, and 10 × 10^{21}/m^3. **b**, **c** The normalized doping concentration-dependent emission power and peak position, respectively

Fig. 7 **a** The calculated spontaneous emission spectra under different pump powers in which the direction of the *arrow* represents the increase of pump power from 5 to 10, 20, 30, 40, 50, 60, 70, 80, 90, and 100 mW. **b** The normalized pump power-dependent emission power

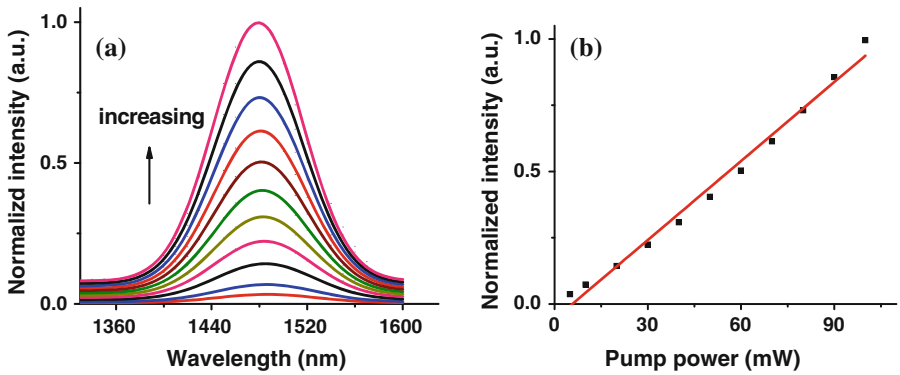

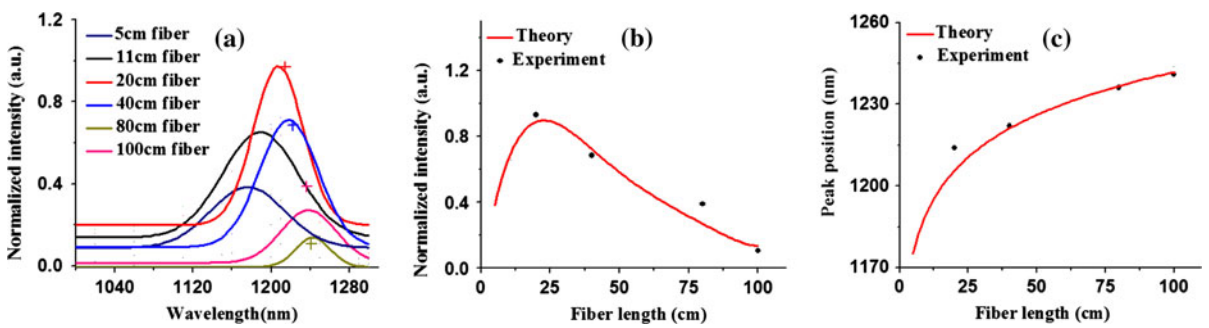

Fig. 8 **a** The calculated emission spectra under different fiber lengths, *plus* (+) represents the experimental results reported by Hreibi et al. (2011). **b** The relationship between the normalized spontaneous emission intensity and the fiber length. **c** The fiber length-dependent experimental and theoretical peak positions

by Hreibi et al. (2011) were employed in this work. The experimental parameters (doping concentration of 1.9 × 10^{22}/m^3, fiber diameter of 25 μm, and QD diameter of 3.5 nm) were adopted for the following theoretical calculations. Figure 8a shows the calculated emission spectra at different fiber lengths from 5 to 100 cm under a fixed pump power of 60 mW; Fig. 8b, c display the normalized fiber length-dependent spontaneous emission power and peak position in both theory and experiment, respectively. The peak position shifted to long wavelength with the increase of the fiber length and the redshift became less for long fibers, not a simple linear relationship. The normalized spontaneous emission power increased first and then

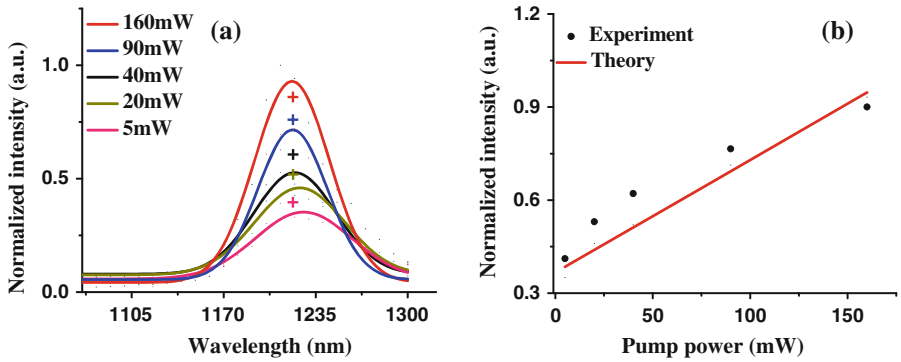

Fig. 9 **a** The calculated emission spectra under different pump powers, *plus* (+) represents the experimental results reported by Hreibi et al. (2011). **b** The pump power-dependent normalized theoretical emission intensity and the experimental data

decreased, which led to an optimal fiber length of 20 cm. The calculated results were close to the experimental data indicating the rationality of the theoretical model.

Figure 9a is the evolution of the spontaneous emission spectrum with different pump powers in a fixed fiber length of 40 cm; Fig. 9b illustrates the relationship of the normalized spontaneous emission intensity and the pump power in both theory and experiment. It is obvious that the normalized emission intensity increases with the increase of the pump power in a nearly linear way and both the theoretical and experimental results are close.

Conclusion

In summary, the theoretical model has been established in this work to investigate the optical properties of multi-mode QD-doped fiber. The emission spectra shifted to long wavelength with the increase of the fiber length, fiber diameter, and doping concentration. The optimum of fiber length, fiber diameter, and doping concentration were achieved separately when other parameters were fixed. The emission increased with the increase of the pump power in a nearly linear way (about 0.0098/mW) in a fiber of 15 cm long and 100 μm diameter with a doping concentration of $4 \times 10^{21}/m^3$. Finally, the spectral properties of 3.5 nm PbSe QD-doped liquid-core fiber were used to confirm the rationality of the above-mentioned theoretical model. This model can be employed to analyze the detailed optical performance of QD-doped fiber, which is applicable to both single- and multi-mode fiber.

Acknowledgments This work was financially supported by the National 863 Program (2011AA050509), the National Natural Science Foundation of China (61106039, 51272084, 61225018, and 11274142), the National Postdoctoral Foundation (2011049015), the Taishan Scholarship, the Hongkong Scholar Program (XJ2012022), the Shandong Natural Science Foundation (ZR2012FZ007), the Jilin Talent Fund, the Jilin Youth Foundation (201101025), and the State Key Laboratory on Integrated Optoelectronics (IOSKL2012ZZ12).

References

An JM, Franceschetti A, Zunger A (2007) The excitonic exchange splitting and radiative lifetime in pbse quantum dots. Nano Lett 7:2129–2135

Bahrampour AR, Rooholamini H, Rahimi L, Askari AA (2009) An inhomogeneous theoretical model for analysis of PbSe quantum-dot-doped fiber amplifier. Opt Commun 282:4449–4454

Cheng C, Zhang H (2007) Characteristics of bandwidth, gain and noise of a PbSe quantum dot-doped fiber amplifier. Opt Commun 277:372–378

Choudhury KR, Sahoo Y, Ohulchanskyy TY, Prasad PN (2005) Efficient photoconductive devices at infrared wavelengths using quantum dot-polymer nanocomposites. Appl. Phys. Lett. 87:073110/1–3

Dai Q, Wang Y, Li X, Zhang Y, Pellegrino DJ, Zhao M, Zou B, Seo J, Wang Y, Yu WW (2009) Size-dependent composition and molar extinction coefficient of PbSe semiconductor nanocrystals. ACS Nano 3:1518–1524

Du H, Chen C, Krishnan R, Krauss TD, Harbold JM, Wise FW, Thomas MG, Silcox J (2002) Optical properties of colloidal PbSe nanocrystals. Nano Lett 2:1321–1324

Ellingson RJ, Beard MC, Johnson JC, Yu P, Micic OI, Nozik AJ, Shabaev A, Efros AL (2005) Highly efficient multiple exciton generation in colloidal PbSe and PbS quantum dots. Nano Lett 5:865–871

Franceschetti A (2008) Structural and electronic properties of PbSe nanocrystals from first principles. Phys Rev B 78:075418/1–6

Giles CR, Desurvire E (1991) Modeling erbium-doped fiber amplifiers. J Lightwave Technol 9:271–283

Harbold JM, Du H, Krauss TD, Cho KS, Murray CB, Wise FW (2005) Time-resolved intraband relaxation of strongly confined electrons and holes in colloidal PbSe nanocrystals. Phys Rev B 72:195312/1–6

Hreibi A, Gerome F, Auguste J, Zhang Y, Yu WW, Blondy J (2011) Semiconductor-doped liquid-core optical fiber. Opt Lett 36:1695–1697

Klimov VI (2006) Mechanisms for photogeneration and recombination of multiexcitons in semiconductornanocrystals: implications for lasing and solar energy conversion. J Phys Chem B 110:16827–16845

Koleilat GI, Levina L, Shukla H, Myrskog SH, Hinds S, Pattantyus-Abraham AG, Sargent EH (2008) Efficient, stable infrared photovoltaics based on solution-cast colloidal quantum dots. ACS Nano 2:833–840

Leitsmann R, Bechstedt F (2009) Characteristic energies and shifts in optical spectra of colloidal IV–VI semiconductor nanocrystals. ACS Nano 3:3505–3512

Lifshitz E, Brumer M, Kigel A, Sashchiuk A, Bashouti M, Sirota M, Galun E, Burshtein Z, Le Quang AQ, Ledoux-Rak I, Zyss J (2006) Air-stable PbSe/PbS and PbSe/PbSe$_x$S$_{1-x}$ core–shell nanocrystal quantum dots and their applications. J Phys Chem B 110:25356–25362

Liljeroth P, van Emmichoven PAZ, Hickey SG, Weller H, Grandidier B, Allan G, Vanmaekelbergh D (2005) Density of states measured by scanning-tunneling spectroscopy shed new light on the optical transitions in pbse nanocrystal. Phys Rev Lett 95:086801/1–4

Lipovskii A, Kolobkova E, Petrikov V, Kang I, Olkhovets A, Krauss T, Thomas M, Silcox J, Wise F, Shen Q, Kycia S (1997) Synthesis and Characterization of PbSe Quantum Dots in Phosphate Glass. Appl Phys Lett 71:3406/1–3

McCumber DE (1964) Theory of phonon-terminated optical masers. Phys Rev 134:A299–A306

McDonald SA, Konstantatos G, Zhang SG, Cyr PW, Klem EJD, Levina L, Sargent EH (2005) Solution-processed PbS quantum dot infrared photodetectors and photovoltaics. Nat Mater 4:138–142

Medintz IL, Goldman ER, Uyeda HT, Mattoussi H (2005) Quantum dot bioconjugates for imaging, labelling and sensing. Nat Mater 4:435–446

Peterka P, Faure B, Blanc W, Karasek W, Dussardier B (2004) Theoretical modelling of S-band thulium-doped silica fibre amplifiers. Opt Quant Electron 36:201–212

Schaller RD, Klimov VI (2004) High Efficiency Carrier Multiplication in PbSe Nanocrystals: Implications for Solar Energy Conversion. Phys. Rev. Lett. 92:186601/1–4

Shabaev A, Efros AIL, Nozik AJ (2006) Multiexciton generation by a single photon in nanocrystals. Nano Lett 6:2856–2863

Steckel JS, Coe-Sullivan S, Bulovic V, Bawendi MG (2003) 1.3 μm to 1.55 μm tunable electroluminescence from PbSe quantum dots embedded within an organic device. Adv Mater 15:1862–1866

Watekar PR, Ju S, Lin A, Kim MJ, Lww BH, Han W-T (2010) Linear and nonlinear optical properties of the PbSe quantum dots doped germano-silica glass optical fiber. J Non-Cryst Solids 356:2384–2388

Wehrenberg BL, Wang C, Sionnest PG (2002) Interband and intraband optical studies of PbSe colloidal quantum dots. J Phys Chem B 106:10634–10640

Weissleder RA (2001) A clearer vision for in vivo imaging. Nat Biotechnol 19:316–317

Wise FW (2000) Lead salt quantum dots: the limit of strong quantum confinement. Acc Chem Res 33:773–780

Yu WW, Qu L, Guo W, Peng X (2003) Experimental determination of the extinction coefficient of CdTe, CdSe, and CdS nanocrystals. Chem Mater 15:2854–2859 (Correction (2004), Chem Mater 16: 560)

Yu WW, Falkner JC, Shih BS, Colvin VL (2004) Preparation and characterization of monodisperse PbSe semiconductor nanocrystals in a noncoordinating solvent. Chem Mater 16:3318–3322